AWARD NUMBER: W81XWH-15-1-0190

TITLE: Neurosteroids Reverse Tonic Inhibition Deficits in Fragile X Syndrome

PRINCIPAL INVESTIGATOR: Dr. Paul A. Davies

CONTRACTING ORGANIZATION: Tufts University School of Medicine
Boston MA 02111-1817

REPORT DATE: August 2016

TYPE OF REPORT: Annual

PREPARED FOR: U.S. Army Medical Research and Materiel Command
Fort Detrick, Maryland 21702-5012

REPORT DOCUMENTATION PAGE

Form Approved
OMB No. 0704-0188

1. REPORT DATE	2. REPORT TYPE	3. DATES COVERED
August 2016	Annual	15 July 2015 – 14 Jul 2016

4. TITLE AND SUBTITLE

Neurosteroids Reverse Tonic Inhibition Deficits in Fragile X Syndrome

5a. CONTRACT NUMBER

5b. GRANT NUMBER
W81XWH-15-1-0190

5c. PROGRAM ELEMENT NUMBER

6. AUTHOR(S)
Dr Paul A. Davies

E-Mail: paul.davies@tufts.edu

5d. PROJECT NUMBER

5e. TASK NUMBER

5f. WORK UNIT NUMBER

7. PERFORMING ORGANIZATION NAME(S) AND ADDRESS(ES)

Tufts University School of
Medicine
136 Harrison Ave
Boston MA 02111-1817

8. PERFORMING ORGANIZATION REPORT NUMBER

9. SPONSORING / MONITORING AGENCY NAME(S) AND ADDRESS(ES)

U.S. Army Medical Research and Materiel Command
Fort Detrick, Maryland 21702-5012

10. SPONSOR/MONITOR'S ACRONYM(S)

11. SPONSOR/MONITOR'S REPORT NUMBER(S)

12. DISTRIBUTION / AVAILABILITY STATEMENT

Approved for Public Release; Distribution Unlimited

13. SUPPLEMENTARY NOTES

14. ABSTRACT
Our preliminary studies demonstrate that Fmr1 KO mice at p21 have a decrease in phosphorylation of S443 in the α4 subunit compared to WT and an increase in the phosphorylation of β3 subunits at the S408/409 site compared to WT. We have previously showed that phosphorylation of these residues changes the trafficking of the subunits so the changes observed in Fmr1 KO mice would predictably have consequences for trafficking of these essential inhibitory subunits. We noted that there was a significant decrease in tonic inhibition in dentate gyrus granule cells in p21 Fmr1 KO mice compared to WT. A 10 min exposure to neuroactive steroids followed by a 30 min wash induced a >3 fold increase in tonic current in Fmr1 KO animals which was prevented with PKC inhibition. Using a perforated multi-electrode array we have observed in cortical-hippocampal slices seizure like events (SLE) propagating through the dentate gyrus and into the CA3 and CA1 regions of the hippocampus of Fmr1 KO mice but in WT mice SLEs did not propagate through the dentate gyrus. We predict the increase neuronal excitability seen in Fmr1 KO mice is due to the deficits in tonic inhibition.

15. SUBJECT TERMS
GABA receptor, protein kinase C (PKC), Neuroactive steroid, tonic inhibition, dentate gyrus, seizures

16. SECURITY CLASSIFICATION OF:			17. LIMITATION OF ABSTRACT	18. NUMBER OF PAGES	19a. NAME OF RESPONSIBLE PERSON
a. REPORT	b. ABSTRACT	c. THIS PAGE			USAMRMC
Unclassified	Unclassified	Unclassified	Unclassified	25	19b. TELEPHONE NUMBER *(include area code)*

Table of Contents

Page

1. Introduction

Fragile X syndrome (FXS) is the most common form of inherited intellectual disability. In addition, there is increased incidence of anxiety, sleep irregularities, and seizure activity. The underlying cause of FXS is a loss of the fragile X mental retardation protein (FMRP). Studies from both FXS patients and animal models have revealed reduced expression levels of extrasynaptic $GABA_AR$ α4 and δ subunits with a reduced efficacy of tonic inhibition. Neuro-active steroids (NAS) are known allosteric modulators of $GABA_AR$ channel function but recent studies from our laboratory have revealed that NAS also exert persistent effects on the efficacy of tonic inhibition by increasing the PKC-mediated phosphorylation of the α4 subunit which increases the membrane expression and boosts tonic inhibition. We have used a combination of biochemical and electrophysiological methods to assess alterations in GABAergic signaling in the hippocampus of FMRP knock-out mouse (*Fmr1 KO*), a widely validated model of the human syndrome. In addition, we propose an innovative way of reversing the reduced tonic inhibition by boosting $GABA_AR$ trafficking to produce a sustained increase in tonic current with the use of NASs including a novel NAS which has improved bioavailability, and pharmacokinetic properties.

2. Keywords

GABA receptor, protein kinase C (PKC), Neuroactive steroid, tonic inhibition, dentate gyrus, seizures

3. Accomplishments

What were the major goals of the project?

Specific Aim 1: Determine the phosphorylated state and cell surface accumulation of $GABA_AR$ subunits in FXS mice and the role of neurosteroids in altering subunit expression.

1. To analyze the NS-mediated changes in phosphorylation of $GABA_ARs$.
2. To test the role that NS exposure plays in regulating the cell surface stability of $GABA_ARs$.

Specific Aim 2. Determining exposure to neurosteroids enhances the efficacy of tonic inhibition in FXS.

1. Measure the efficacy for NS to rescue the deficits of tonic inhibition in *Fmr1 KO* mice.
2. Characterize the changes to phasic inhibition in dentate gyrus from *Fmr1 KO* mice.
3. To examine the deficit of tonic inhibition on circuit excitability in *Fmr1 KO* mice compared to WT and impact of NS treatment.

Specific Aim 3. Ascertaining behavioral phenotypes in *Fmr1 KO* mice will be reversed with NS exposure.

1. To examine audiogenic seizures in *Fmr1 KO* mice following NS treatment.

2. To compare inappropriate social behavior in *Fmr1 KO* and WT mice.

• Milestone #1: Manuscript on the findings from the study. 18-24 months of study. 50% completion.

What was accomplished under these goals?

We have published our findings on phosphorylation of S408/409 residues on the β3 subunit in the *Fmr1 KO* mouse in Vien et al., 2015. The β3 subunit, along with α4 subunits, are major subunits contributing to extrasynaptic $GABA_A$Rs. Phosphorylation of these residues decreases the endocytosis of $GABA_A$Rs containing the β3 subunit. We assessed the importance of these residues by creating a mouse with the residues mutated to alanines (S408/9A) which also reduces endocytosis. The mouse exhibited autistic like properties such as increased repetitive behavior, decreased social interaction, and altered dendritic spine morphology. Because of the comorbidity of seizures in autism we examined seizure activity in the S408/9A mouse. The mice exhibited increase sensitivity to kainic acid-induced seizures. Similar to our preliminary findings in the *Fmr1 KO* mouse, the S408/9A mouse also had reduced tonic currents and increased phasic currents in dentate gyrus granule cells. Furthermore, we observed a decrease in α4 subunit immunoreactivity in hippocampal sections from S408/9A mouse. These data demonstrate that changes in the phosphorylation of β3 subunits can alter $GABA_A$R expression and contribute to the pathophysiology of autistic spectrum disorders.

Data for Specific Aim 1. *Determine if the alterations in the phosphorylation state of $GABA_A$R subunits in Fmr1 KO mice impacts the cellular distribution within the hippocampus.* We have previously shown that there are reductions in the phosphorylation of $GABA_A$R α4 subunits. Because these changes can affect the trafficking of $GABA_A$Rs in the membrane we examined the cellular distribution of the α4 subunit. We stained 40 μm hippocampal slices with antibodies against the α4 subunit together with antibodies against the inhibitory postsynaptic inhibitory protein gephyrin. Using confocal microscopy coupled with *Metamorph* analysis we examined the α4 subunit/gephyrin positive puncta in the dentate gyrus between genotypes. As illustrated in Fig. 1, there appeared to be an increase in α4 subunit immunoreactivity at gephyrin positive structures in the brains of *Fmr1 KO* mice.

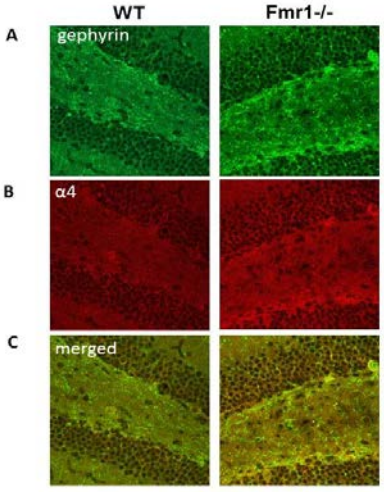

Figure 1. Characterization of α4-containing inhibitory synapses in Fmr1 KO. *40μm hippocampal slices were stained with antibodies against the $GABA_A$R α4 subunit and gephyrin, a marker of inhibitory synapses. The number of α4/gephyrin positive puncta was compared within the dentate gyrus between genotypes. In Fmr1 KO mice, the number of α4 colocalized with gephyrin increased, consistent with an increase in the altered localization of α4-containing $GABA_A$Rs to inhibitory synapses.*

NASs increase the phosphorylation and cell surface stability of $GABA_ARs$

We have previously shown that the naturally occurring NAS, THDOC, increased tonic current in part through phosphorylation of S408/409 of the β3 subunit (Abramian et al., 2014; Vien et al., 2015). To further our understanding of the NAS-mediated increase in tonic current we measured the effects of ALLO, and SGE-516 on the phosphorylation and membrane expression of β3 subunits in hippocampal slices. Twenty min exposure to 100nM ALLO, or SGE-516 increased phosphorylation of β3 subunits at S408/409 to 141 ± 10% of control (n=10, p<0.01), and 143 ± 14% of control (n=4, p<0.05) respectively (Fig. 2A&B).

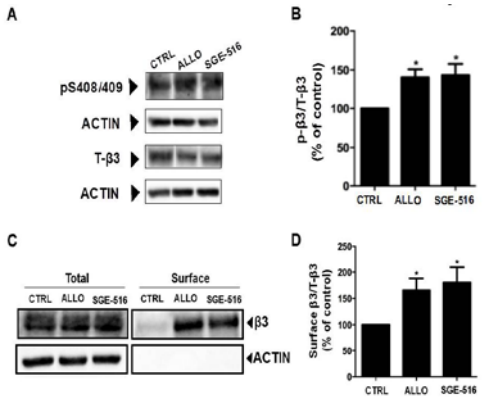

Figure 2. NAS exposure increases phosphorylation and surface expression of β3 subunits. ***A.*** *Exposure to 100 nM of the NASs, ALLO or SGE-516, for 20 min increases β3 S408/409 phosphorylation in acute hippocampal slices.* ***B.*** *The ratio of p-β3/T-β3 was measured and values were normalized to those in control (100%). Asterisks represent a significant difference from control (ALLO: p <0.01, Student's t test, n=10; SGE-516: p<0.05, Student's t test, n=4).* ***C.*** *Exposure to 100 nM ALLO or SGE-516 for 20 min increases $GABA_A$-β3–containing receptors at the plasma membrane in acute hippocampal slices.* ***D.*** *The ratio of surface β3/T-β3 was measured and values were normalized to cell surface levels in control treated slices (100%). Asterisks represent a significant difference from control (ALLO: p <0.05, Student's t test, n=8; SGE-516: p<0.05, Student's t test, n=4).*

In parallel with modulating phosphorylation, exposure to 100 nM ALLO, or SGE-516 increased the cell surface expression levels of receptors containing β3 subunits to 166 ± 22% of control (n=8, p<0.05), and 180 ± 29% of control (n=4, p<0.05) respectively (Fig. 2C&D). Therefore, in parallel with inducing sustained effects on GABAergic inhibition ALLO and SGE-516 enhance the cell surface levels and phosphorylation of the $GABA_ARs$ containing β3 subunits dependent upon PKC activity

Specific Aim2.

Measuring the efficacy of NAS to increase tonic current. We analyzed the sustained effects of ALLO, or the new synthetic NAS SGE-516 on the tonic current in DGGCs in hippocampal slices from 3-5 week old C57 male mice. Hippocampal slices were incubated for 15 min in a chamber containing NASs dissolved in ACSF. Slices were then transferred to the recording chamber of the microscope followed by a wash period between 30 to 60 mins of continuous perfusion of NAS-free ACSF before recordings were started (Fig. 3A).

Slices exposed to ALLO, or SGE-516 demonstrated a concentration-dependent increase in the tonic current measured by the addition of picrotoxin with the maximal effects at 1 μM. Control, vehicle-treated slices had a tonic current of 43.6 ± 5.7 pA (n=12), whereas the tonic currents for slices treated

with SGE-516 (1 μM) was 123.0 ± 22.2 pA, (n=6, p= 0.0003), or ALLO (1 μM) was 95.8 ± 10.8 pA (n=4, p= 0.0005, Fig. 3B&C).

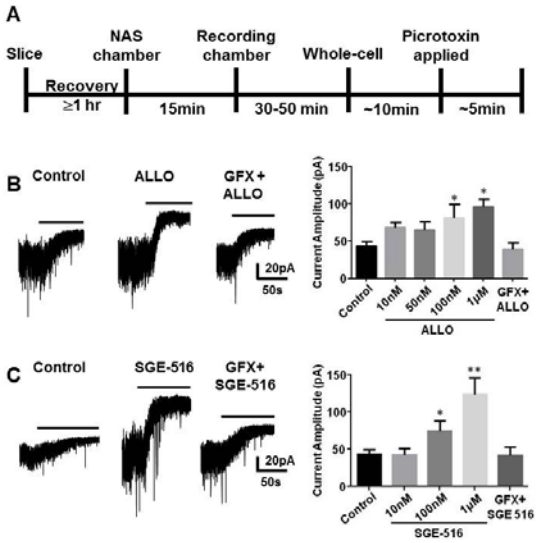

Figure 3. NAS-mediated metabotropic enhancement of tonic inhibitory current in DGGC neurons. A. *Scheme demonstrating experimental protocol. Hippocampal slices were allowed to recover for at least 1 hr following slicing. Slices were then incubated for 15 min in a chamber containing NASs dissolved in ACSF. Slices were then transferred to the recording chamber of the microscope followed by a wash period between 30 to 60 min of continuous perfusion of NAS-free ACSF before recordings were started. Recordings were made from DGGCS in hippocampal slices from p21-35 C57 mice in the presence of 1 μM GABA followed by 100 μM picrotoxin and the difference in holding current was then determined.* ***Left panel B & C.*** *Example tonic currents from slices following exposures to vehicle (control) or 100 nM ALLO (B), 100 nM SGE-516 (C) for 15 min. No change in tonic current was observed in slices pre-incubated for 15 min with GFX followed by ALLO, or SGE-516. Bar above current represents application of picrotoxin (100μM).* ***Right panel B & C.*** *Bar graph shows average tonic current was significantly enhanced following exposure to different concentrations of ALLO and SGE-516. In all panels * = significantly different to control (p<0.05; t-test, n=4-12 cells).*

To analyze the efficacy of phasic inhibition of Fmr1 KO mice. As noted before, IPSC biophysical properties changed in the *Fmr1 KO* mouse, with the IPSC amplitude increasing and the decay prolonging compared to wild-type. The data presented above shows an increase in α4 subunit immunoreactivity at gephyrin positive structures in the hippocampus suggesting the α4 subunit at synapses. We have assessed the effects of the benzodiazepine diazepam (which enhance αβγ2 $GABA_A$Rs where α can be 1-3 subunits) on sIPSC amplitude, and decay in WT and *Fmr1 KO* mice. Additionally, we have examined the α4βγ2 specific benzodiazepine Ro15-4513 on sIPSC properties between genotypes.

In wild type mice, diazepam significantly enhanced IPSC amplitude and prolonged decay whereas in *Fmr1 KO* mice only decay was prolonged (Fig 4A&B). Conversely, in the presence of Ro15-4513, IPSC amplitude and decay where unchanged in wild type mice but were significantly enhanced in the *Fmr1 KO* mice (Fig 4C&D).

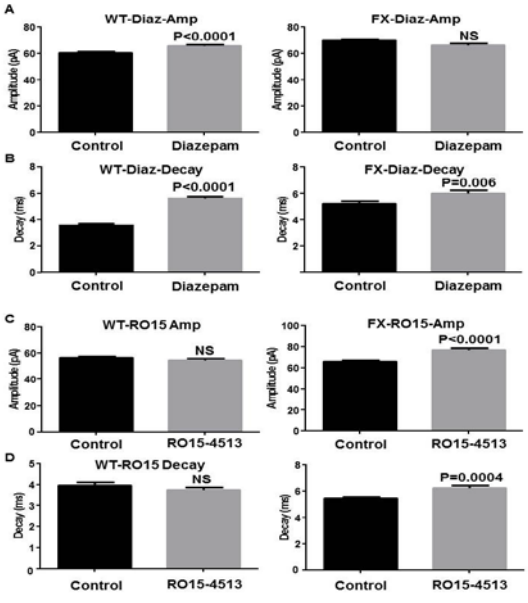

Figure 4. Modulation of DGGC IPSCs by benzodiazepines. *Recordings were made from DGGCs in hippocampal slices from p21-35 WT, or Fmr1 KO mice. Fmr1 KO mice displayed larger sIPSC amplitudes and longer decay times compared to age-matched controls.* Bar graphs show the effects of acute (10min) exposures to diazepam (A&B) or Ro15-4513 (C&D) applied to slices from wild-type (left column) and Fmr1 KO (right column) mice.

These data suggest the involvement of α4 subunit in synaptic $GABA_A$Rs. This is a new finding in the FXS field and could explain the poor clinical effects of benzodiazepines because α4 subunits are insensitive to the modulation by most benzodiazepines.

To examine the impact of modified GABAergic inhibition on circuit excitability in Fmr1 KO mice. We have examined the circuit excitability of the hippocampus using a perforated multi-electrode array (pMEA) system. A deficit in tonic current observed in *Fmr1 KO* mice is hypothesized to reduce tonic inhibition which would increase the overall circuit excitability by increasing the likelihood of neurons to fire action potentials. It has been proposed that in FXS there is an increase in neuronal excitability and synchrony across various brain structures (Goncalves et al 2013). Our preliminary data demonstrating a reversal of the tonic current deficit in *Fmr1 KO* with NS treatment would be expected to restore tonic inhibition and reduce the excessive circuit excitability.

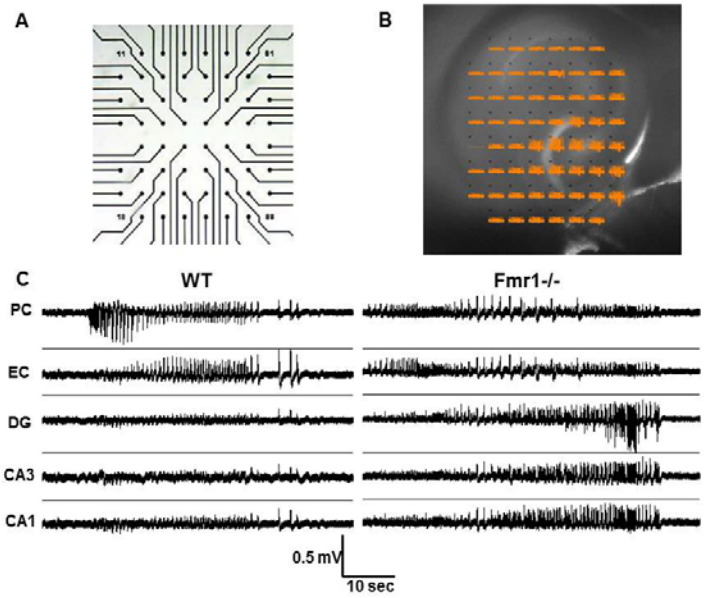

Figure 5. In vitro seizure like events (SLE) in hippocampal slices from WT and Fmr1 KO mice in the absence of Mg^{+2} using multi-electrode array (MEA) system. *Hippocampal slices from Fmr1 KO and WT mice were tested for seizure like events (SLE) in absence of Mg^{+2} using MEA.* ***A.*** *Multi-electrode array chamber* ***B.*** *MEA-layout (iii). Typical slice on MEA-layout (iv) MEA stage & amplifier.* ***C.*** *Traces showing the first SLEs from the dentate gyrus (DG), CA3 neurons (CA3), CA1 neurons (CA1), entorhinal cortex (EC), postrhinal cortex (PC) regions of the hippocampal slices from WT and Fmr1 KO mice.*

Seizure-like events (Padgett et al) were induced by low Mg^{2+} artificial cerebrospinal fluid (ACSF) to relieve the Mg^{2+} block of NMDA receptors (Traub et al 1994).

We obtained preliminary data with a pMEA on loan from the supplier. We recorded field potentials from horizontal cortical-hippocampal slices from WT and *Fmr1 KO* mice (Fig.5B). SLEs were induced by perfusing the recording chamber with low Mg^{2+} ACSF. SLEs were characterized by tonic-clonic discharges, with an initial tonic phase followed by a period of clonic after-discharges. Interestingly, we observed a dramatic regional difference in SLE propagation (Fig. 5C). In the WT slices, the first SLE occurred in the entorhinal cortex (EC) and postrhinal cortex (PC) but did not show full propagation through the dentate gyrus (DG). In contrast, the first SLEs in *Fmr1 KO* slices propagated through the DG, indicating an increased potential susceptibility of DG recruitment during onset of epileptiform activity in slices from *Fmr1 KO* mice. The DG is known to be important for epileptogenesis because it forms the so-called dentate-gate that prevents activity spreading from cortex to the hippocampus. Tonic inhibition in the dentate gyrus seems to be critical in preventing excessive neuronal excitability.

What opportunities for training and professional development has the project provided?

Dr. Amit Modgil participates in lab meetings, presenting data on a regular basis. Amit will also present his findings to the whole Neuroscience Department once a year in our post-doctoral research seminar series. He also attends weekly department seminars. In addition the postdoctoral program at Tufts runs a weekly career development seminar series. Speakers in this series are drawn from the local pharmaceutical and biotechnology industry in the local area, which highlights the range of career opportunities for life scientist with doctoral degrees. He also attends didactic and tutorial courses related to animal care and use, laboratory safety, radiation safety and the responsible conduct of research.
Dr Amit Modgil was selected to give an oral presentation at the Gordan Research Seminar for "Fragile X and Autism-Related Disorders". Dr Modgil also presented a poster at the Gordan Research Conference for "Fragile X and Autism-Related Disorders" in Vermont, June 2016.

How were the results disseminated to communities of interest?

Dr Modgil and Dr Davies presented a poster at the "Neuro Developmental Disorders symposium" at Harvard Medical School, October 2015.
Dr Amit Modgil gave an oral presentation at Gordan Research Seminar for "Fragile X and Autism-Related Disorders". Dr Modgil and Dr Davies presented posters at the Gordan Research Conference for "Fragile X and Autism-Related Disorders" in Vermont, June 2016.

What do you plan to do during the next reporting period to accomplish the goals?

Specific Aim 1. We plan to examine how exposure to NASs affect $GABA_AR$ subunit phosphorylation and surface expression in *Fmr1 KO* mice. Particularly, we will examine if NAS exposure restores the surface expression and cellular distribution to extrasynaptic sites.

Specific Aim 2. We plan to examine the concentration-dependent increase in tonic current with NAS exposure in *Fmr1 KO* mice. Following this, we will examine how that rise in tonic current influences circuit excitability.

Specific Aim 3. We will examine seizure susceptibility and social behavior in *Fmr1 KO* mice treated with vehicle or NAS.

4. Impact

What was the impact on the development of the specific discipline(s) of the project?

The α4 subunits are usually thought to be located extrasynaptically mediating tonic inhibition. In FXS it is believed that the expression of α4 subunit containing $GABA_A$Rs is reduced, thereby decreasing the contribution of tonic inhibition to the overall inhibition in neurons resulting in excessive excitation. However, our data has suggested that the change in phosphorylation of subunits in *Fmr1 KO* mice leads to a redistribution of subunits which cause a reduction of tonic current and an alteration of phasic inhibition. The relocation of the α4 subunit, in particular, to synaptic sites not only alters phasic current biophysics it also changes the pharmacological response to benzodiazepines. This has not been observed before in FXS models and can help explain the lack of benzodiazepine efficacy in FXS. Our data also point to tonic inhibition contributing significantly to the "dentate gate", an important characteristic of the dentate gyrus in limiting excessive neuronal activity flowing into the hippocampus and out back into the cortex.

What was the impact on other disciplines?

The breakdown of the dentate gate because of the redistribution of the α4 subunit and reduction of tonic current will impact the knowledge in the epilepsy field.

What was the impact on technology transfer?

This project could impact the therapeutic targets used by pharmaceutical companies. Most GABAergic compounds to date have been developed as positive allosteric modulators. However, this project indicates that mechanisms which influence trafficking of subunits would be a valid therapeutic target.

What was the impact on society beyond science and technology?

Nothing to report.

5. Changes/Problems

SGE-797 has been re-formulated to make it available orally and has been re-named SGE-516.
Some results examined the phosphorylation of β3 subunits. Some temporally technical problems arose with the antibody to the α4 subunit, so we progressed the project with the antibody to the β3 subunit.

6. Products

Publications resulting from the work under this award:

Vien TN, Modgil A, Abramian AM, Jurd R, Walker J, Brandon NJ, Terunuma M, Rudolph U, Maguire J, **Davies PA**, Moss SJ. Compromising the phosphodependent regulation of the GABAAR β3 subunit

reproduces the core phenotypes of autism spectrum disorders. Proc Natl Acad Sci U S A. 2015;112:14805-14810. Published; acknowledged federal support.

Modgil A, Parakala ML, Ackley MA, Doherty JJ, Moss SJ, **Davies PA**. Endogenous and synthetic neuroactive steroids evoke sustained increases in the efficacy of GABAergic inhibition via a protein kinase C-dependent mechanism. Neuropharmacology 2016; under review; acknowledged federal support.

Other publications during reporting period:

Nakamura Y, Morrow DH, Modgil A, Huyghe D, Deeb TZ, Lumb MJ, **Davies PA**, Moss SJ. Proteomic Characterization of Inhibitory Synapses Using a Novel pHluorin-tagged γ-Aminobutyric Acid Receptor, Type A (GABAA), α2 Subunit Knock-in Mouse. J Biol Chem. 2016;291:12394-407. Published; acknowledged federal support.

7. Participants & Other Collaborating Organizations

What individuals have worked on the project?

Name:	Paul A. Davies
Project Role:	co-PI, Initiating PI
Researcher Identification (ORCID ID):	0000-0002-3973-3143
Nearest person month worked:	3 calendar months
Contribution to Project:	Has designed experiments and performs analysis and interpretation of the results. He also supervises other members of the research team and is responsible for writing reports and producing manuscripts.
Funding Support:	NIH-NIMH R01 MH097446

Name:	Stephen J. Moss
Project Role:	co-PI
Researcher Identification:	
Nearest person month worked:	0.5 calendar months
Contribution to Project:	Supervising the experiments designed to assay the effects of neurosteroids on $GABA_AR$ phosphorylation and cell surface accumulation.

Funding Support: NIH-NIDA DA037170-01, NIH-NIMH R01 MH097446, NIH-NINDS R01 NS081986, NIH-NINDS, 1R01NS087662, AstraZeneca; IMED/$GABA_BR$ drug development.

Name: Amit Modgil
Project Role: Postdoctoral Researcher
Researcher Identification:
Nearest person month worked: 6 calendar months
Contribution to Project: Has performed the electrophysiology experiments, making hippocampal slices and examining the effects of their exposure to neurosteroids.
Funding Support: Funded from R01 MH097446

Name: Manasa L. Parakala
Project Role: Graduate student
Researcher Identification:
Nearest person month worked: 6 calendar months
Contribution to Project: Has performed the biochemistry experiments examining $GABA_AR$ phosphorylation and cell surface accumulation.
Funding Support: Funded from R01 MH097446

Has there been a change in the active other support of the PD/PI(s) or senior/key personnel since the last reporting period?

Nothing to report

What other organizations were involved as partners?

Organization Name: SAGE Therapeutics

Location of Organization: Cambridge, MA

Partner's contribution to the project:

Collaboration. SAGE Therapeutics share the necessary proprietary compounds and data necessary to support the success of this project

8. Special Reporting Requirements

Collaborative Award

9. Appendices

Vien TN, Modgil A, Abramian AM, Jurd R, Walker J, Brandon NJ, Terunuma M, Rudolph U, Maguire J, Davies PA, Moss SJ. Compromising the phosphodependent regulation of the GABAAR β3 subunit reproduces the core phenotypes of autism spectrum disorders. Proc Natl Acad Sci U S A. 2015;112:14805-14810.

Compromising the phosphodependent regulation of the $GABA_AR$ β3 subunit reproduces the core phenotypes of autism spectrum disorders

Thuy N. Vien[a], Amit Modgil[a], Armen M. Abramian[a], Rachel Jurd[a], Joshua Walker[a], Nicholas J. Brandon[b], Miho Terunuma[c], Uwe Rudolph[d], Jamie Maguire[a], Paul A. Davies[a], and Stephen J. Moss[a,e,1]

[a]Department of Neuroscience, Tufts University School of Medicine, Boston, MA 02111; [b]AstraZeneca Neuroscience iMed, Cambridge, MA 02139; [c]Department of Cell Physiology and Pharmacology, University of Leicester, Leicester LE1 9HN, United Kingdom; [d]Laboratory of Genetic Neuropharmacology, McLean Hospital, and Department of Psychiatry, Harvard Medical School, Belmont, MA 02478; and [e]Department of Neuroscience, Physiology, and Pharmacology, University College, London WC1E 6BT, United Kingdom

Edited by Richard L. Huganir, The Johns Hopkins University School of Medicine, Baltimore, MD, and approved October 22, 2015 (received for review July 24, 2015)

Alterations in the efficacy of neuronal inhibition mediated by $GABA_A$ receptors ($GABA_ARs$) containing β3 subunits are continually implicated in autism spectrum disorders (ASDs). In vitro, the plasma membrane stability of $GABA_ARs$ is potentiated via phosphorylation of serine residues 408 and 409 (S408/9) in the β3 subunit, an effect that is mimicked by their mutation to alanines. To assess if modifications in β3 subunit expression contribute to ASDs, we have created a mouse in which S408/9 have been mutated to alanines (S408/9A). S408/9A homozygotes exhibited increased phasic, but decreased tonic, inhibition, events that correlated with alterations in the membrane stability and synaptic accumulation of the receptor subtypes that mediate these distinct forms of inhibition. S408/9A mice exhibited alterations in dendritic spine structure, increased repetitive behavior, and decreased social interaction, hallmarks of ASDs. ASDs are frequently comorbid with epilepsy, and consistent with this comorbidity, S408/9A mice exhibited a marked increase in sensitivity to seizures induced by the convulsant kainic acid. To assess the relevance of our studies using S408/9A mice for the pathophysiology of ASDs, we measured S408/9 phosphorylation in *Fmr1* KO mice, a model of fragile X syndrome, the most common monogenetic cause of ASDs. Phosphorylation of S408/9 was selectively and significantly enhanced in *Fmr1* KO mice. Collectively, our results suggest that alterations in phosphorylation and/or activity of β3-containing $GABA_ARs$ may directly contribute to the pathophysiology of ASDs.

GABA receptor | phosphorylation | autism spectrum disorder | tonic inhibition | phasic inhibition

$GABA_A$ receptors ($GABA_ARs$) are Cl^- selective ligand-gated ion channels that mediate phasic and tonic inhibition in the adult brain. Consistent with their roles in limiting neuronal excitability, benzodiazepines, barbiturates, general anesthetics, and neurosteroids exert their anxiolytic, anticonvulsant, hypnotic, and sedative effects via potentiating $GABA_AR$ activity (1). $GABA_ARs$ are heteropentamers constructed from α1–6, β1–3, γ1–3, δ, ε, θ, and π subunits. Phasic inhibition is principally mediated by receptors assembled from α1–3, β1–3, and γ2 subunits, whereas those receptors that mediate tonic inhibition contain α4–6, β1–3, and δ subunits (2). Studies using KO mice have shown that the β3 subunit is an essential component of receptor subtypes that mediate phasic and tonic inhibition (3). Together with the *Fmr1* gene (Fragile X mental retardation), mutations to the 15q11–13 locus, where the $GABA_AR$ β3 gene resides, are the leading monogenetic causes of autism spectrum disorders (ASDs) (4). Moreover, β3 subunit mutations have been described in seizure disorders, and alterations in subunit expression levels have also been reported in ASDs (3, 5).

In vitro studies have revealed that the β3 subunit plays a critical role in regulating the plasma membrane accumulation and synaptic targeting of $GABA_ARs$ via phosphorylation of the intracellular serine residues 408 and 409 (S408/9) (6, 7). S408/9 are substrates of cAMP-dependent PKA, PKC, Ca^{2+}-calmodulin type 2-dependent protein kinases (Cam KIIs), and cGMP-dependent protein kinase, and they are principally dephosphorylated by protein phosphatase 2A (8). S408/9 are the principal mediators of high-affinity binding to the clathrin adaptor molecule AP2 within the β3 subunit, and thereby facilitate $GABA_AR$ endocytosis (9). Phosphorylation of S408/9 reduces the affinity of the β3 subunit for AP2 by 100-fold, and mutation of S408/9 to alanine residues (S408/9A) has been shown to mimic the effects of phosphorylation on AP2 binding to the β3 subunit (9, 10). Accordingly, overexpression of the mutant β3 S408/9A subunit in cultured hippocampal neurons leads to an increase in the number and size of inhibitory synapses (7).

Studies in animal models of ASDs have reported modifications in the expression levels of some $GABA_AR$ mRNAs and proteins (11, 12). However, the mechanisms underlying these alterations in subunit expression and if they contribute to ASDs remain to be addressed. Therefore, in this study, we have analyzed the role that modified β3 subunit phosphorylation may play in the pathophysiology of ASDs. To test this role, we created a

Significance

Alterations in the efficacy of neuronal inhibition mediated by $GABA_A$ receptors ($GABA_ARs$) containing β3 subunits are continually implicated in autism spectrum disorders (ASDs). In vitro, the plasma membrane stability of $GABA_ARs$ is potentiated via phosphorylation of serine residues 408 and 409 (S408/9) in the β3 subunit, an effect that is mimicked by their mutation to alanines. Here, we created a mouse in which S408/9 have been mutated to alanines (S408/9A). S408/9A mice exhibited altered dendritic spine structure, increased repetitive behavior, decreased social interaction, and an epileptic phenotype. Thus, mutation of S408/9 reproduces the core deficits seen in humans with ASDs. Collectively, our results suggest that alterations in phosphorylation and/or activity of β3-containing $GABA_ARs$ may directly contribute to the pathophysiology of ASDs.

Author contributions: T.N.V., A.M., A.M.A., R.J., J.W., M.T., U.R., and J.M. designed research; T.N.V., A.M., A.M.A., R.J., J.W., N.J.B., M.T., U.R., and J.M. performed research; A.M.A., M.T., and U.R. contributed new reagents/analytic tools; T.N.V., A.M., A.M.A., R.J., J.W., N.J.B., M.T., U.R., J.M., and P.A.D. analyzed data; and T.N.V., N.J.B., U.R., J.M., P.A.D., and S.J.M. wrote the paper.

Conflict of interest statement: S.J.M. serves as a consultant for AstraZeneca and SAGE Therapeutics, relationships that are regulated by Tufts University and do not have an impact on this study.

This article is a PNAS Direct Submission.

[1]To whom correspondence should be addressed. Email: stephen.moss@tufts.edu.

This article contains supporting information online at www.pnas.org/lookup/suppl/doi:10.1073/pnas.1514657112/-/DCSupplemental.

mouse in which the principal sites of phosphodependent regulation within the receptor β3 subunit, S408/9, have been mutated to S408/9A, a mutation that mimics the effects of their phosphorylation. S408/9A mice exhibited increased phasic but decreased tonic inhibition events, which correlated with alterations in the membrane stability of the receptor subtypes that mediate these distinct forms of inhibition. S408/9A mice exhibited alterations in dendritic spine structure, increased repetitive-like behavior, and decreased social interaction, which are hallmarks of ASDs. Therefore, our results provide evidence that alterations in the activity of $GABA_A$Rs containing β3 subunits directly contribute to ASDs.

Results

Creation of a S408/9A Knock-In Mouse. Alterations in the efficacy of GABAergic inhibition mediated by β3-containing $GABA_A$Rs are strongly linked to ASDs. Phosphorylation of $GABA_A$Rs regulates their exocytosis and endocytosis, and thereby their residence time on the neuronal plasma membrane and accumulation at inhibitory synapses (8). Central to these regulatory processes is the phosphorylation of S408/9 in the β3 subunit, which reduces the affinity of $GABA_A$Rs for the clathrin adaptor protein AP2, as measured by using synthetic peptides corresponding to the β3 subunit and purified AP2 (9, 13). The significance of these findings has recently been questioned by studies that suggest that the arginine residues flanking S408/9 are the principal determinants of AP2 binding in the β3 subunit (14). To examine the significance of S408/9 further, we expressed the intracellular domain of the β3 subunit as a GST fusion protein (GSTβ3) or a fusion protein in which the respective residues were mutated to alanines (GSTβ3S408/9A) in *Escherichia coli.* The respective fusion proteins were then phosphorylated in vitro using purified PKC to final stoichiometries of ∼0.35 and ∼0.03 mol/mol, respectively, and then exposed to the μ2 subunit of AP2 (15) (Fig. S1*A*). Phosphorylation of GSTβ3 significantly reduced μ2 binding, whereas phosphorylation of GSTβ3S408/9A was without effect. Likewise GSTβ3S408/9A bound significantly lower levels of μ2 compared with GSTβ3. Collectively, these results suggest a key role for S408/9 and their phosphorylation in determining the affinity of $GABA_A$Rs for AP2 (Fig. S1 *A* and *B*).

To assess the significance of β3 subunit phosphorylation in determining the efficacy of GABAergic inhibition, we created a knock-in mouse in which S408/9 were mutated to S408/9A using homologous recombination in ES cells (Fig. S1 *C* and *D*). Mutation of the respective codons in exon 9 of the β3 subunit was confirmed by DNA sequencing (Fig. S1 *C* and *D*), and the respective mice were backcrossed on the C57BL/6J background in excess of 10 generations. S408/9A homozygotes were viable and bred normally and did not exhibit any overt phenotypes. Likewise, there did not appear to be any gross anatomical changes in the structure of the hippocampus (Fig. S1*E*). In hippocampal slices from WT mice, treatment with the PKC activator phorbol 12,13-dibutyrate produced a large increase in pS408/9 immunoreactivity, an effect not replicated in S408/9A mice (Fig. 1*A*). To control for possible global changes in $GABA_A$R phosphorylation mice, we analyzed phosphorylation of Y367 in the γ2 subunit, an accepted substrate of Src family kinases (16). Treatment of slices with vanadate, an inhibitor of tyrosine phosphatases, induced similar increases in Y367 phosphorylation in WT and S408/9A mice (Fig. 1*A*).

Characterization of $GABA_A$R expression levels and synaptic targeting in S408/9A mice. Next, we examined the effects of the S408/9A mutation on the cell surface accumulation of the $GABA_A$Rs using biotinylation. The S408/9A mutation increased the cell surface expression levels of the β3 subunit to 145 ± 8% of WT ($P < 0.05$, $n = 4$ mice of each genotype; Fig. 1*B*) without modifying total subunit expression levels ($P > 0.05$, $n = 4$ mice of each genotype; Fig. 1*C*). In the dentate gyrus, phasic inhibition is mediated by $GABA_A$R assembled from of α1/2, β2, β3, and γ2 subunits, whereas subtypes containing α4–6, β2, β3, and δ subunits are responsible for tonic current. Therefore, we assessed the effects of the S408/9 mutation on the plasma membrane accumulation of the receptor α2 and α4 subunits. The plasma membrane levels of the α2 subunit were increased in S408/9A mice to 119.0 ± 5.2% of control ($P < 0.05$, $n = 5$–6 mice of each genotype; Fig. 1*B*). In

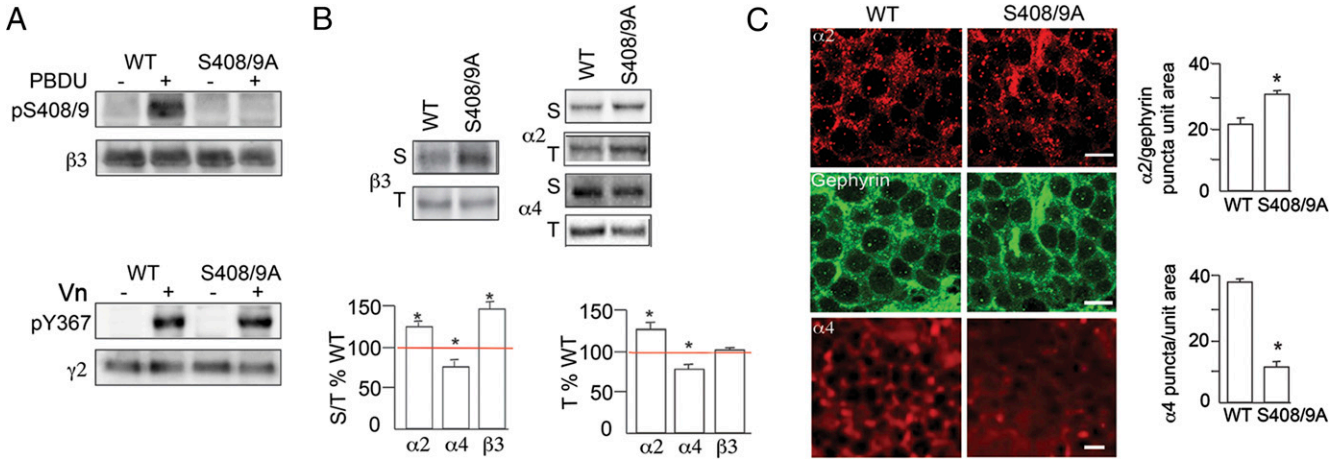

Fig. 1. $GABA_A$R expression in S408/9A mice. (*A*) Treatment of hippocampal slices from WT mice with 100 nM phorbol 12,13-dibutyrate (PDBU) increased pS408/9 immunoreactivity consistent with published studies demonstrating that both residues are substrates of PKC (8). In contrast, pS408/9 immunoreactivity was not detected in S408/9A mice. (*B*) Biotinylation revealed that the surface levels of the β3 subunits, along with the synaptic α2 subunits, were increased in the S408/9A mice, whereas surface accumulation of $GABA_A$Rs containing α4 subunits was decreased. Hippocampal slices were subjected to biotinylation, followed by immunoblotting with anti-α2, anti-α4, and anti-β3 subunit antibodies. The ratio of surface/total (S/T%WT) was measured in S408/9A mice and WT control mice, and values were then normalized to WT controls (100%, red line). Total expression levels were also compared between genotypes (T%WT). *Significantly different from control ($P < 0.05$, *t* test; $n = 5$–6 mice of each genotype). (*C*) Forty-micron hippocampal slices were stained with antibodies against the α2 and α4 subunits and gephyrin fluorescent-conjugated secondary antibodies, followed by confocal microscopy. The number of α2/gephyrin-positive puncta and α4 puncta was then compared within the dentate gyrus between genotypes. Preventing phosphorylation of the β3 subunit increases the number of inhibitory synapses in the dentate gyrus of the hippocampus but reduces α4 puncta immunoreactivity. *Significantly different from control ($P < 0.001$, *t* test; $n = 3$ mice of each genotype). (Scale bars: 10 μm.)

contrast, the α4 subunit was decreased to 81.0 ± 4.5% of levels seen in WT ($P < 0.05$, $n = 6$ mice of each genotype; Fig. 1*B*). These changes in cell surface accumulation were mirrored by parallel changes in increased total expression levels of the α2 subunits and decreased total expression levels of the α4 subunits to 120.7 ± 4.3% and 85.3 ± 7.0%, respectively, compared with WT controls ($P < 0.05$, $n = 4$–8 mice of each genotype; Fig. 1*B*).

To characterize the subcellular distribution of $GABA_A$Rs in S408/9A mice, hippocampal sections were subjected to immunohistochemistry with antibodies against $GABA_A$R α2 or α4 subunits. In some experiments, sections were also stained with antibodies against the inhibitory scaffold protein gephyrin. Sections were then visualized using confocal microscopy, and subunit expression levels were quantified within the dentate gyrus. The number of inhibitory synapses defined as α2/gephyrin puncta were increased in S408/9A mice compared with WT littermates (23.4 ± 2.5 vs. 32.0 ± 0.6 for WT and S408/9A mice, respectively; $P < 0.05$, $n = 3$ mice of each genotype; Fig. 1*C*). In contrast, the number of puncta of α4 subunit immunoreactivity was decreased (13.1 ± 1.2 vs. to 37.4 ± 0.8 puncta per 2,500 μm^2 for S408/9A and WT mice, respectively; $P < 0.001$; Fig. 1*C*). Additionally, in contrast to the effects seen with $GABA_A$Rs, the levels of gephyrin, postsynaptic density protein-95, and the AMPA receptor subunit GluA1 were unaffected by the S408/9A mutation (Fig. S2).

Collectively, these results reveal that S408/9A mice have deficits in the cell surface accumulation of $GABA_A$Rs that mediate tonic inhibition but an increased level of those $GABA_A$Rs that mediate phasic inhibition.

S408/9A exhibited an increase in phasic inhibition and decreased tonic current. To examine the functional significance of the alterations in $GABA_A$R expression seen in S408/9A mice, we used patch-clamp recording to analyze GABAergic inhibition in dentate gyrus granule cells (DGGCs). In DGGCs from S408/9A mice, tonic current was significantly decreased (24.7 ± 4.1 vs. 11.9 ± 2.2 pA for WT and S408/9A mice, respectively; $P < 0.005$, $n = 10$–11 cells, three mice of each genotype; Fig. 2*A*). In contrast, the amplitude of spontaneous inhibitory postsynaptic currents (sIPSCs) was significantly increased in S408/9A mice compared with WT controls (28.4 ± 2.4 vs. 42.5 ± 3.3 pA for WT and S408/9A mice, respectively; $P < 0.005$, $n = 17$–18 cells, three mice of each genotype; Fig. 2*B*). However, the frequency (4.5 ± 0.2 vs. 4.4 ± 0.1 Hz for WT and S408/9A mice, respectively) and decay time (44.7 ± 12.8 vs. 24.8 ± 2.5 ms for WT and S408/9A mice, respectively; $P > 0.05$, $n = 17$–18 cells, three mice of each genotype) of sIPSCs was comparable between genotypes.

We also assessed the impact of the modifications in GABAergic inhibition on neuronal excitability. First, we compared the properties of excitatory postsynaptic currents (EPSCs) in DGGCs. In S408/9A mice, EPSC amplitude was significantly increased (14.6 ± 1.05 vs. 18 ± 1.02 pA for WT and S408/9A mice, respectively; $P < 0.05$; Fig. 2*C*) with no difference in frequency (1.4 ± 0.3 vs. 1.3 ± 0.2 Hz for WT and S408/9A mice, respectively). Moreover, their decay was also prolonged (2.1 ± 0.1 vs. 2.4 ± 0.2 ms for WT and S408/9A mice, respectively; $P < 0.05$, $n =$ 14–16 cells, three mice of each genotype). However, net excitability of DGGCs and their resting membrane potentials were not modified by the S408/9A mutation ($n = 19$–20 cells, three mice of each genotype; Fig. 2*D* and Table S1).

Therefore, S408/9A mice have reduced tonic but enhanced phasic inhibition, but these changes do not lead to any gross changes in neuronal excitability, presumably because S408/9A mice also exhibit elevations in EPSC amplitude.

S408/9A Mice Exhibit Deficits in Social Interaction and Increased Repetitive Behavior. ASDs have a common core of behavioral deficits, including reduced social interaction and increased repetitive behavior. Therefore, we assessed if any of these parameters are altered in S408/9A mice. First, we assessed if the respective mutation modifies motor coordination as measured using the rotarod, a critical control for data interpretation in rodent behavioral experiments. The latency to fall in the rotarod test was not different at 16–32 rpm in S408/9A mice compared with WT mice (Fig. S3*A*). Likewise, there were no differences between genotypes for the total distance traveled or dwell time in the center of the open field (Fig. S3 *B* and *C*). We also compared anxiety-like behavior using the light/dark test. WT and S408/9A mice spent equivalent time in the light chamber (46.9 ± 2.2% vs. 41.8 ± 2.5% for WT and S408/9A mice, respectively; $P > 0.05$, $n = 12$ mice of each genotype; Fig. S3*D*).

Social behavior was measured using the two-choice and three-chamber social interaction test. In the two-choice assay, WT controls spent more time in the chamber containing the novel mouse than in the chamber containing the empty cage, whereas S408/9A mice had no preference for the novel mouse over the

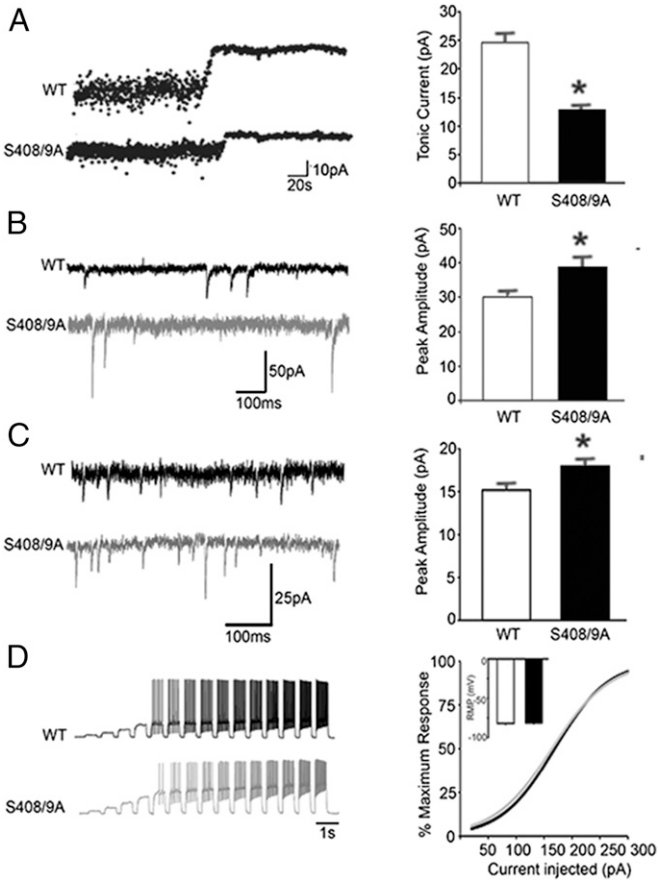

Fig. 2. Characterization of phasic and tonic inhibition in S408/9A mice. (*A*) Tonic conduction is decreased in S408/9A mice. Tonic current in DGGCs was compared between genotypes in the presence and absence of gabazine. The tonic current amplitude of S408/9A mice was significantly smaller than tonic current amplitude of WT mice. *Significantly different from control ($P < 0.01$, *t* test; $n = 10$–11 cells, three mice of each genotype). (*B*) sIPSCs were recorded from DGGCs of WT mice (black) and S408/9A mice (gray) *Significantly different from WT control ($P < 0.001$, *t* test; $n = 17$–18 cells, three mice of each genotype). (*C*) Examples of EPSCs recorded from DGGCs of WT mice (black) and S408/9A mice (gray) *Significantly different from control ($P <$ 0.05, *t* test; $n = 14$–16 cells, three mice of each genotype). (*D*) Representative recordings of action potential firing in DGGCs from WT mice (black) and S408/9A mice (gray) in response to 0.5-s current injections from 20 to 300 pA in 20-pA increments. Average input/output curves from DGGCs from WT mice (black) and S408/9A mice (gray) are shown as a Boltzmann function generated by the averages of the fitted parameters. (*Inset*) No difference in the resting membrane potential (RMP) was observed between genotypes. Values are mean ± SEM ($n = 19$–21 cells, three mice of each genotype).

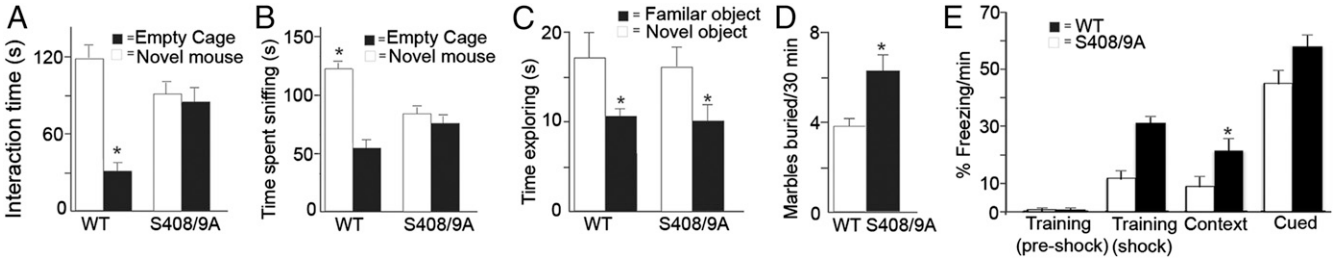

Fig. 3. Characterization of social interaction and repetitive-like behavior in S408/9A mice. (*A*) Preference for an empty cage or novel mouse was determined in a two-choice social interaction setup. *Significantly different from control ($P < 0.01$, ANOVA with Tukey's post hoc comparison; $n = 12$ mice of each genotype). (*B*) Three-chamber social interaction assay was used to measure the preference for a novel mouse or an empty cage. The amount of time mice spent in a predefined sniffing zone around the empty cage or novel mouse was digitally tracked. *Significantly different from control ($P < 0.001$, ANOVA with Tukey's post hoc comparison; $n = 12$–16 mice of each genotype). (*C*) Preference for a familiar object or a novel object was determined for the genotypes. *Significantly different from control ($P < 0.05$, ANOVA with Tukey's post hoc comparison; $n = 10$–12 mice of each genotype). (*D*) Repetitive-like behavior was assessed using the marble burying assay. ($P < 0.01$, *t* test; $n = 18$–19 mice of each genotype). (*E*) Learning and memory were assessed using the fear-conditioning assay. The percentage of freezing per minute was assessed during training and for context-dependent and cued-dependent learning. *Significantly different from control ($P < 0.05$, *t* test; $n = 12$–13 mice of each genotype).

empty cage (time spent interacting with empty cage: 49.8 ± 7.4 s (WT), 86.6 ± 17.6 s (S408/9A); time spent interacting with novel mouse: 119.4 ± 19.0 s (WT), 92.7 ± 17.7 s (S408/9A); $n = 12$ mice of each genotype, $P < 0.01$; Fig. 3*A*). Consistent with the profound deficits in social interaction observed in the two-choice assay, S408/9A mice exhibited no preference for the novel mouse in the three-chamber social interaction assay. WT controls spent more time in the novel mouse sniffing zone than in the empty cage sniffing zone (time spent interacting with empty cage: 55.4 ± 5.8 s (WT), 71.9 ± 8.4 s (S408/9A); time spent interacting with novel mouse: 123.8 ± 5.1 s (WT), 85.7 ± 6.9 s (S408/9A); $n = 12$–16 mice of each genotype, $P < 0.01$; Fig. 3*B*). In contrast, S408/9A mice showed no preference for the novel mouse over an empty cage, consistent with ASD-like deficits in social interaction. As a control for our measurements for social preference, we examined the ability of S408/9A mice to discriminate between a novel object and a familiar object. Both WT controls and S408/9A mice spent more time interacting with the novel object (66 ± 0.9% vs. 64 ± 7.7% of total time for WT and S408/9A mice, respectively; $P < 0.05$, $n = 10$–11 mice of each genotype; Fig. 3*C*).

To measure repetitive-like behavior in S408/9A mice, we used the marble burying assay. S408/9A mice displayed an increase in repetitive-like behavior in the marble burying test (6.0 ± 0.6 marbles in 30 min compared with 3.8 ± 0.5 marbles in WT controls; $P < 0.001$, $n = 18$–19 mice of each genotype; Fig. 3*D*). Therefore, S408/9A mice exhibited an increase in repetitive-like behavior and deficits in social interaction, which are behavioral characteristics commonly observed in ASDs.

Finally, we assessed if the S408/9A mutation has an impact on cognition by comparing contextual and cued fear conditioning between genotypes. S408/9A mice exhibited enhanced context-dependent learning (training: 11.8 ± 3.0% freezing per minute (WT), 32.1 ± 4.3% freezing per minute (S408/9A); $P > 0.05$; context: 8.9 ± 3.4% freezing per minute (WT), 21.4 ± 4.2% freezing per minute (S408/9A); $P < 0.05$; Fig. 3*E*) compared with WT controls but no statistical differences in cue-dependent learning (cued: 45.1 ± 6.6% freezing per minute (WT), 60.8 ± 6.4% freezing per minute (S408/9A); $P > 0.05$; Fig. 3*E*).

S408/9A Mice Have Increased Seizure Susceptibility. ASDs are frequently comorbid with epilepsy. Therefore, we analyzed the impact of the S408/9A mutation on seizure susceptibility. Mice were implanted with EEG electrodes, and seizures were induced with 20 mg/kg of kainic acid and monitored to ensure seizures reached stage 3–4 on the Racine scale (forelimb clonus and rearing with forelimb clonus). Representative EEG traces during epileptiform events captured 30 min after kainic acid injection illustrate a marked increase in epileptiform activity in S408/9A mice over WT controls (Fig. 4*A*). Strikingly, S408/9A mice exhibited a faster onset to the first epileptiform event compared with WT mice (4.6 ± 0.7 vs. 11.2 ± 1.1 min of latency for S408/9A and WT mice, respectively; $P < 0.001$, $n = 8$–10 mice of each genotype; Fig. 4*B*). Additionally, S408/9A mice entered status epilepticus at an earlier time point than WT controls (41.8 ± 4.3 vs. 61.5 ± 8.6 min for S408/9A and WT mice, respectively; $P < 0.05$, $n = 8$–10 mice of each genotype; Fig. 4*B*). Furthermore, S408/9A mice spent a greater percentage of the total time experiencing epileptiform activity compared with WT controls (82.5 ± 2.1% vs. 65.4 ± 6.4% for S408/9A and WT mice, respectively; $P < 0.05$, $n = 8$–10 mice of each genotype; Fig. 4*B*). Therefore, the S408/9A mutation significantly increases seizure susceptibility.

S408/9A Mice Exhibited Increased Hippocampal Dendritic Spine Density. Alterations in spine structure are a common feature in ASDs (17). Therefore, we assessed if the alterations in GABAergic inhibition have an impact on dendritic structure. Brains from both genotypes were subjected to Golgi staining and visualized using stereology. We quantified the density of spines along 30-μm-long sections of

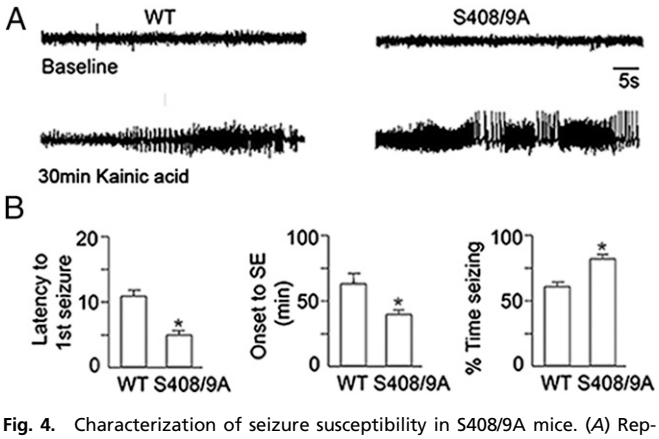

Fig. 4. Characterization of seizure susceptibility in S408/9A mice. (*A*) Representative EEG traces for WT and S408/9A mice at baseline and 30 min after kainic acid injection. (*B*) Latency to the first epileptiform activity, onset of status epilepticus (SE), and total time experiencing epileptiform activity were digitally tracked and measured. S408/9A mice had a shorter latency to the first epileptiform activity, faster onset of status epilepticus, and spent a great percentage of time experiencing epileptiform activity compared with WT controls. *Significantly different from control ($P < 0.05$, *t* test; $n = 8$–10 mice of each genotype).

dendrites in the molecular layer above the dentate gyrus of the hippocampus. In S408/9A mice, a pronounced increase in spine density was seen (28.6 ± 0.7 vs. 34.8 ± 1.0 per 30-μm dendrite for WT and S408/9A mice, respectively; $P < 0.0001$, $n = 12$ neurons in three independent experiments; Fig. 5*A*). Similarly, the spines in S408/9A mice appeared to be more filopodia-like in structure compared with their equivalents in WT mice, and some exhibited pronounced branching. Therefore, S408/9A mice displayed similar abnormalities in spine structure to those abnormalities reported in *Fmr1* KO mice and patients with ASDs.

S408/9A Phosphorylation Is Increased in *Fmr1* KO (Fragile X Syndrome) Mice. To assess the relevance of our studies further, we measured S408/9 phosphorylation in *Fmr1* KO mice, a model of Fragile X syndrome (FXS). S408/9 phosphorylation was significantly increased to 285.6 ± 24.3% in *Fmr1* KO mice compared with WT controls ($P < 0.005$; $n = 3$ mice of each genotype; Fig. 5*B*). In contrast to S408/9, phosphorylation of S383 was similar in *Fmr1* KO mice compared with WT controls ($P > 0.05$, $n = 3$ mice of each genotype; Fig. 5*B*).

Discussion

Deficits in the efficacy of neuronal inhibition mediated by $GABA_A$Rs containing the β3 subunit are widely believed to contribute to the pathophysiology of ASDs. Accordingly, modifications in $GABA_A$R β3 subunit gene structure and/or protein expression levels, together with both deletions and duplications of the 15q11–13 locus, are leading causes of ASDs (5, 18).

In vitro studies have shown that phosphorylation of S408/9 regulates the cell surface stability and synaptic accumulation of β3-containing $GABA_A$Rs (7), and, here, we have analyzed the significance of this putative regulatory process for the pathophysiology of ASDs. To do so, we created a S408/9A knock-in mouse using homologous recombination. S408/9A mice were viable and did not exhibit any overt phenotypes or gross alterations in the structure of the hippocampus. Consistent with the lowered affinity for AP2 in the S408/9A mutation in vitro, the cell surface expression levels of the β3 subunit in the hippocampus were increased in S408/9A mice compared with WT controls. Within the dentate gyrus, the β3 subunit assembles with the α2/γ2 or α4/δ subunits to form $GABA_A$R subtypes that mediate phasic and tonic inhibition, respectively (2). Strikingly, in the dentate gyrus of S408/9A mice, there was a significant increase in the expression levels of the α2 subunit and the number of inhibitory synapses. In contrast, deficits in the expression levels of the α4 subunit were seen. Thus, in addition to membrane trafficking, S408/9 and/or their phosphorylation may play a role in regulating the assembly of individual $GABA_A$R subtypes. Significantly, our findings of alterations in α4 and β3 subunit expression are consistent with GABAergic dysfunction in *Mecp2* and *Fmr1* KO mice, which are accepted models of ASDs (11, 19, 20).

Consistent with this result, the amplitude of sIPSCs was increased and their decay was slowed in DGGCs from S408/9A mice. In contrast, a reciprocal decrease in the cell surface accumulation of the α4 subunit was seen in S408/9A mice, which paralleled a reduction in tonic current. The gross excitability of DGGCs as measured by current injection was not altered between strains, reflecting the increase in EPSC amplitude in S408/9A mice. Therefore, preventing the phosphodependent modulation of the $GABA_A$Rs by mutating S408/9 in the β3 subunit to alanines alters the equilibrium between phasic and tonic inhibition in the dentate gyrus.

Previous in vitro studies have suggested that for synaptic $GABA_A$Rs containing α1/2β3γ2 subunits, mutation of S408/9A does not compromise receptor assembly, or transport to the plasma membrane, but selectively reduces their endocytosis (9). Therefore, the increased synaptic accumulation of the α2 subunit in S408/9A mice presumably results from their enhanced residence time on the plasma membrane. In contrast to synaptic receptors, the mechanisms that control the membrane trafficking of receptors containing α4 subunits are less well defined. However, it is evident from our results that phosphorylation of S408/9 may play opposing roles in regulating the assembly and membrane trafficking of α4 subunit containing $GABA_A$Rs to those roles established for subtypes that mediate phasic inhibition. Clearly, further studies are required to identify the role that S408/9 and their phosphorylation plays in regulating the differential membrane trafficking of $GABA_A$R subtypes that mediate phasic and tonic inhibition.

In parallel with these modifications in GABAergic inhibition, the number of dendritic spines was strikingly increased in the mutant mice. Significantly, overexpressing S408/9A cDNA in cultured hippocampal neurons leads to similar changes in spine maturity to those changes seen in S408/9A mice (7). It is emerging that tonic inhibition plays a central role in reducing neuronal excitability, particularly at depolarizing membrane potentials (21). Given the emerging role for tonic inhibition in regulating neuronal output, the deficits in the efficacy of this process in S408/9A mice may lead to prolonged neuronal depolarization and enhanced intracellular Ca^{2+} signaling, which would be predicted to have significant effects on spine architecture.

In addition to modifications in dendritic structure, ASDs have a common core of behavioral symptoms, including increased repetitive behavior and anxiety, together with deficits in social interaction (17). Therefore, we compared these parameters between genotypes. Compared with WT controls, S408/9A mice exhibited decreased social interaction as measured in both the two-choice and three-chamber assays; however, S408/9A mice and WT controls

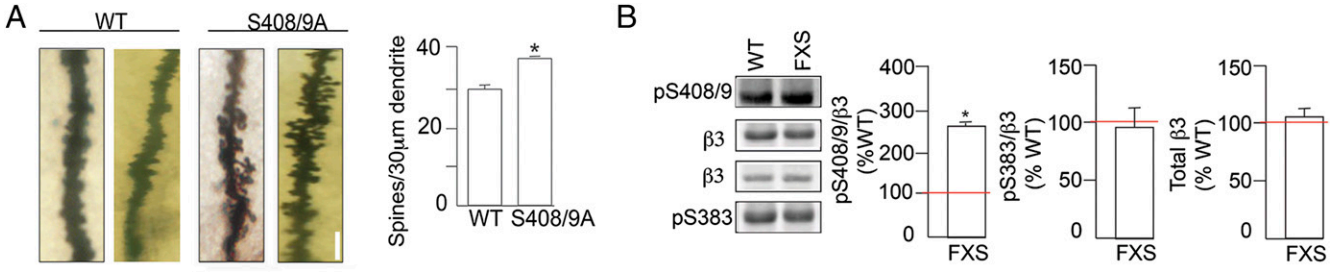

Fig. 5. Characterization of dendritic spine density in DGGCs from S408/9A mice and β3 phosphorylation in *Fmr1* KO (FXS) mice. (*A*) Representative dendrites from DGGCs of two different mice. (Scale bar: 2 μm.) The number of spines per 30 μm of dendrite was then determined and compared between genotypes. *Significantly different from control ($n = 12$ neurons from three independent experiments, three mice of each genotype; $P < 0.0001$, *t* test). (*B*) Hippocampal lysates from WT and *Fmr1* KO mice on a FVB/N (Friend leukemia virus B strain) background were subjected to SDS/PAGE and immunoblotted with pS408/9, pS383, and β3 subunit antibodies. The pS408/9/β3 or pS383/β3 ratios in *Fmr1* KO mice (FXS) were normalized to WT controls (100%; red line). *Significantly different from control ($P < 0.01$, *t* test; $n = 3$ mice of each genotype).

shared a similar preference for a novel object over a familiar object. S408/9A mice also exhibited an increase in repetitive-like behavior as measured using the marble burying assay. Significantly, the mutation did not alter locomotor activity, behavior in the open field, or behavior in the light/dark test. S408/9A mice did not appear to exhibit any modifications in anxiety. ASDs are often comorbid with epilepsy, and consistent with this comorbidity, S408/9A mice exhibit increased sensitivity to kainate-induced seizures. Thus, although the changes in phasic and tonic inhibition seen in S408/9A mice do not appear to lead to changes in net neuronal excitability, they are important determinants of epileptogenesis. Finally, we noted that in the *Fmr1* KO mouse model of FXS, specific alterations in S408/9 phosphorylation were seen. The mechanism linking deficits in FMRP expression and enhanced S408/9 phosphorylation requires further experimentation. However, it is interesting to note that FMRP is part of a signaling complex that contains protein phosphatase 2A (PP2A), the principle phosphatase that dephosphorylates S408/9 (10, 22, 23). Thus, deficits in FMRP expression levels may affect the stability and/or subcellular targeting of PP2A, leading to reduced rates of S408/9 dephosphorylation.

In conclusion, our results suggest that alterations in the phosphorylation status of $GABA_AR$ β3 resulting in compromised GABAergic inhibition are central to the pathophysiology of FXS. Therefore, restoring the efficacy of tonic inhibition may be a useful therapeutic strategy to alleviate the burdens of ASDs.

Materials and Methods

All protocols were approved by Tufts University's Institutional Animal Care and Use Committee and were conducted in accordance with the NIH *Guide for the Care and Use of Laboratory Animals* (24). More detailed information on materials and methods is provided in *SI Materials and Methods*.

Creation of the S408/9A Mice. The S408/9A mice were created using homologous recombination as detailed previously (25).

Biochemical Measurements. Antibodies used in this study have been described previously, as have the methods for immunoblotting and immunoprecipitation (22, 26).

Electrophysiology and EEG Recordings. Phasic and tonic inhibition was measured using the patch-clamp technique (27). The Pinnacle Technology system and LabChart (ADInstruments) were used for EEG recordings and analysis as previously described (28).

Behavior. Measurements using the rotarod and activity in the open field and anxiety were assessed as described previously (26).

ACKNOWLEDGMENTS. We thank Jay Boltax and Hew Mun Lau (McLean Hospital) for technical assistance in generating the mutant allele in ES cells. This work was supported by Grant 206026 from the Simons Foundation (to S.J.M.); NIH–National Institute of Neurological Disorders and Stroke Grants NS051195, NS056359, NS081735, R21NS080064, and NS087662 (to S.J.M.); NIH–National Institute of Mental Health Grant MH097446 (to P.A.D. and S.J.M.); and US Department of Defense Grant AR140209 (to P.A.D. and S.J.M.). J.M. is supported by Grant NS073574, and U.R. is supported by Grant R01MH080006.

1. Rudolph U, Möhler H (2006) GABA-based therapeutic approaches: GABAA receptor subtype functions. *Curr Opin Pharmacol* 6(1):18–23.
2. Brickley SG, Mody I (2012) Extrasynaptic GABA(A) receptors: Their function in the CNS and implications for disease. *Neuron* 73(1):23–34.
3. DeLorey TM, et al. (1998) Mice lacking the beta3 subunit of the GABAA receptor have the epilepsy phenotype and many of the behavioral characteristics of Angelman syndrome. *J Neurosci* 18(20):8505–8514.
4. Abrahams BS, Geschwind DH (2008) Advances in autism genetics: On the threshold of a new neurobiology. *Nat Rev Genet* 9(5):341–355.
5. Delahanty RJ, et al. (2011) Maternal transmission of a rare GABRB3 signal peptide variant is associated with autism. *Mol Psychiatry* 16(1):86–96.
6. Brandon NJ, et al. (1999) Synaptic targeting and regulation of GABA(A) receptors. *Biochem Soc Trans* 27(4):527–530.
7. Jacob TC, et al. (2009) GABA(A) receptor membrane trafficking regulates spine maturity. *Proc Natl Acad Sci USA* 106(30):12500–12505.
8. Nakamura Y, Darnieder LM, Deeb TZ, Moss SJ (2015) Regulation of GABAARs by phosphorylation. *Adv Pharmacol* 72:97–146.
9. Kittler JT, et al. (2005) Phospho-dependent binding of the clathrin AP2 adaptor complex to GABAA receptors regulates the efficacy of inhibitory synaptic transmission. *Proc Natl Acad Sci USA* 102(41):14871–14876.
10. Terunuma M, et al. (2008) Deficits in phosphorylation of GABA(A) receptors by intimately associated protein kinase C activity underlie compromised synaptic inhibition during status epilepticus. *J Neurosci* 28(2):376–384.
11. Martin BS, Corbin JG, Huntsman MM (2014) Deficient tonic GABAergic conductance and synaptic balance in the fragile X syndrome amygdala. *J Neurophysiol* 112(4):890–902.
12. DeLorey TM (2005) GABRB3 gene deficient mice: A potential model of autism spectrum disorder. *Int Rev Neurobiol* 71:359–382.
13. Jacob TC, Moss SJ, Jurd R (2008) GABA(A) receptor trafficking and its role in the dynamic modulation of neuronal inhibition. *Nat Rev Neurosci* 9(5):331–343.
14. Smith KR, et al. (2012) Stabilization of GABA(A) receptors at endocytic zones is mediated by an AP2 binding motif within the GABA(A) receptor β3 subunit. *J Neurosci* 32(7):2485–2498.
15. Moss SJ, Doherty CA, Huganir RL (1992) Identification of the cAMP-dependent protein kinase and protein kinase C phosphorylation sites within the major intracellular domains of the beta 1, gamma 2S, and gamma 2L subunits of the gamma-aminobutyric acid type A receptor. *J Biol Chem* 267(20):14470–14476.
16. Jurd R, Tretter V, Walker J, Brandon NJ, Moss SJ (2010) Fyn kinase contributes to tyrosine phosphorylation of the GABA(A) receptor gamma2 subunit. *Mol Cell Neurosci* 44(2):129–134.
17. Hutsler JJ, Zhang H (2010) Increased dendritic spine densities on cortical projection neurons in autism spectrum disorders. *Brain Res* 1309:83–94.
18. Kang JQ, Barnes G (2013) A common susceptibility factor of both autism and epilepsy: Functional deficiency of GABA A receptors. *J Autism Dev Disord* 43(1):68–79.
19. Olmos-Serrano JL, et al. (2010) Defective GABAergic neurotransmission and pharmacological rescue of neuronal hyperexcitability in the amygdala in a mouse model of fragile X syndrome. *J Neurosci* 30(29):9929–9938.
20. Chao HT, et al. (2010) Dysfunction in GABA signalling mediates autism-like stereotypies and Rett syndrome phenotypes. *Nature* 468(7321):263–269.
21. Wlodarczyk AI, et al. (2013) Tonic GABAA conductance decreases membrane time constant and increases EPSP-spike precision in hippocampal pyramidal neurons. *Front Neural Circuits* 7:205.
22. Jovanovic JN, Thomas P, Kittler JT, Smart TG, Moss SJ (2004) Brain-derived neurotrophic factor modulates fast synaptic inhibition by regulating GABA(A) receptor phosphorylation, activity, and cell-surface stability. *J Neurosci* 24(2):522–530.
23. Narayanan U, et al. (2007) FMRP phosphorylation reveals an immediate-early signaling pathway triggered by group I mGluR and mediated by PP2A. *J Neurosci* 27(52):14349–14357.
24. Committee on Care and Use of Laboratory Animals (1996) *Guide for the Care and Use of Laboratory Animals* (Natl Inst Health, Bethesda), DHHS Publ No (NIH) 85-23.
25. Terunuma M, et al. (2014) Postsynaptic GABAB receptor activity regulates excitatory neuronal architecture and spatial memory. *J Neurosci* 34(3):804–816.
26. Tretter V, et al. (2009) Deficits in spatial memory correlate with modified gamma-aminobutyric acid type A receptor tyrosine phosphorylation in the hippocampus. *Proc Natl Acad Sci USA* 106(47):20039–20044.
27. Kretschmannova K, et al. (2013) Enhanced tonic inhibition influences the hypnotic and amnestic actions of the intravenous anesthetics etomidate and propofol. *J Neurosci* 33(17):7264–7273.
28. Lee V, Maguire J (2013) Impact of inhibitory constraint of interneurons on neuronal excitability. *J Neurophysiol* 110(11):2520–2535.

Supporting Information

Vien et al. 10.1073/pnas.1514657112

SI Materials and Methods

Mice. Ten- to 12-wk-old male S408/9A mice and the corresponding WT littermates were housed in a 12-h light/dark cycle with standard rodent food and water ad libitum. For behavioral testing, animals were acclimatized to the testing room for 1 h before the start of all procedures.

***Gabrb3* (Gene That Encodes for the β3 $GABA_AR$ Subunit Protein).** S408/9A mice were generated by gene targeting in murine ES cells using standard techniques. Briefly, a targeting vector was constructed containing 7.4 kb of homologous genomic sequence (from 3 kb upstream of the 5′ end of exon 9 to 4.4 kb downstream of the 5′ end of exon 9). The genomic DNA was subcloned from a substrain 129S5 BAC, obtained from the Wellcome Trust Sanger Institute. In exon 9 (the final exon), the codons for S408/9 of the $GABA_AR$ β3 subunit were mutated to alanine codons (S408/9A). A *lox*P-flanked neomycin expression cassette (*lox*P-FRT-PGKneobpA-FRT-SA-4xSv40pA-SD-*lox*P) was inserted 0.3 kb upstream of the 5′ end of exon 9. An HSV-TK (herpes simplex virus-thymidine kinase) cassette for negative selection was positioned 3′ of the homology. The NotI-linearized targeting vector was electroporated into TC-1 ES cells (derived from substrain 129S6, a gift from Phil Leder, Department of Genetics, Harvard Medical School, Belmont, MA). Correctly targeted clones were identified by PCR and sequenced to verify the double-point mutation and the loxP sites, and they were injected into C57BL/6J mouse blastocysts. Chimeric male mice were bred with WT C57BL/6J females, and the entire neomycin expression cassette was excised by Cre/*lox*P-mediated recombination. Mice were backcrossed to C57BL/6J for a minimum of 10 generations. Experimental animals were derived from heterozygous breedings. The proposed allele symbol for the β3-S408/9A allele in the MGI database is $Gabrb3^{tm2Uru}$.

Antibodies. Polyclonal rabbit antibodies against α2, α4, β2, and δ were gifts from Verena Tretter and Werner Sieghart (both from Medical University Vienna, Vienna). Anti-β3 and anti–phospho-β3 (phospho-S408/9 and phospho-S383) antibodies were generated and verified by the S.J.M. laboratory (9, 10, 12). The following antibodies were purchased from commercial vendors: monoclonal anti-α1 (clone N95/35; NeuroMab), monoclonal anti-gephyrin (catalog no. 147011; Synaptic Systems), and monoclonal anti-actin (catalog no. A2228; Sigma–Aldrich).

Western Blot. Standard Western blotting protocols were used as previously described (10). Briefly, hippocampi were rapidly dissected, flash-frozen, and lysed in lysis buffer composed of the following: 20 mM Tris·HCl (pH 8.0), 150 mM NaCl, 1% Triton X-100, 5 mM EDTA, 10 mM NaF, 2 mM Na_3VO_4, 10 mM pyrophosphate, 0.1% SDS, and 50 mM NaF. Total protein concentration was established, and 40 μg of hippocampal lysate was subjected to SDS/PAGE, transferred to nitrocellulose membranes, and blocked with 5% (wt/vol) BSA in Tris-buffered saline-Tween 20 for 1 h. Membranes were immunoblotted with the indicated primary antibodies, and following extensive rinsing, they were probed with HRP-conjugated secondary antibodies and detected with enhanced chemiluminescence. Blots were imaged, and data were normalized to actin and quantified with the CCD-based LAS 3000 system (FujiFilm).

Surface Biotinylation. Three hundred fifty-micron-thick hippocampal slices from 10- to 12-wk-old male WT control (C57BL/6) mice or age-matched male S408/9A mice were prepared on a vibratome (Leica VT1000S) in cold, oxygenated artificial cerebral spinal fluid (ACSF) composed of 124 mM NaCl, 3 mM KCl, 25 mM $NaHCO_3$, 2 mM $MgSO_4$, 2 mM $CaCl_2$, 1.1 mM NaH_2PO_4, and 10 mM glucose (pH 7.4). After sectioning, slices were allowed a 1-h recovery period in oxygenated, ice-cold ACSF. Following the recovery period, slices were incubated for 30 min at 4 °C with 1 mg/mL NHS-SS-biotin (Pierce). Following three rinses in ice-cold ACSF to remove excess biotin, hippocampal samples were lysed. After adjusting for protein concentration, hippocampal lysates were incubated with streptavidin beads (Pierce) overnight at 4 °C. Bound substances were subjected to SDS/PAGE, followed by immunoblotting with the indicated antibodies. Immunoblots were quantified using the CCD-based LAS 3000 system. For phospho-specific antibodies, the ratio of phospho-β3/total-β3 was calculated and S408/9A values were normalized to WT control (100%).

EEG Recordings. EEGs were performed as previously described (28). Age-matched male littermates, aged 10–12 wk, were used for recording EEGs in awake, behaving animals. Mice were deeply anesthetized and implanted with prefabricated head mounts containing six-pin connectors with two electromyogram reference electrodes (Pinnacle Technology) 2.0 mm posterior to the bregma, along the midsagittal suture, and 2 mm below the dura. Following a 1-wk recovery period, EEG activity was monitored using the Pinnacle Technology turnkey system with a 100× amplifier and were high-pass-filtered at 1.0 Hz (PowerLabs; ADInstruments). A 30-min baseline was obtained before an i.p. injection of 20 $mg{\cdot}kg^{-1}$ kainic acid (Tocris), followed by continuous EEG monitoring for an additional 120 min. Epileptiform activity was defined as electrographic events with amplitudes greater than twofold the standard deviation of the averaged baseline that last a minimum of 10 s and are separated from another event by greater than 10 s. Epileptiform activity was additionally confirmed by an increase in the power and frequency of high-amplitude events. Latency to the first seizure was defined as the time from injection of kainic acid until the first electrographic seizure. Duration of epileptiform activity was calculated from the cumulative time in minutes of epileptiform activity divided by 120 min. The onset of status epilepticus was defined as epileptiform activity lasting longer than 5 min with no silent period greater than 10 s. Duration of epileptiform activity, latency to the first epileptiform event, and latency to onset of status epilepticus were quantified using LabChart, version 7 (ADInstruments).

Immunohistochemistry. Ten- to 12-wk-old male mice were perfused intracardially with 4% (wt/vol) paraformaldehyde, brains were dissected and immersed in 30% (wt/vol) sucrose for 72 h, and 40-μm-thick sections were prepared from fresh-frozen tissue using a microtome. Free-floating sections were processed for immunohistochemistry. Tissue was extensively rinsed in BupH-PBS (Thermo Fisher Scientific) and blocked for 1 h in 10% (wt/vol) BSA with 0.3% Triton X-100 in BupH-PBS. Tissue was incubated overnight at room temperature with the indicated antibodies, extensively rinsed in BupH-PBS, and incubated for 2 h in Alexa Fluor 488 and/or Alexa Fluor 568 secondary antibodies (Life Technologies, Thermo Fisher Scientific). After extensive rinsing with BupH-PBS, tissues were mounted, dried, and coverslipped with ProLong Gold anti-fade reagent with DAPI (Invitrogen). Images were obtained with a Nikon Ti microscope and analyzed with

ImageJ (NIH) software. Controls consisted of incubating slices in the absence of primary antibody.

Electrophysiology. The brains of male mice were rapidly dissected and placed in oxygenated, ice-cold ACSF solution containing 225 mM sucrose, 2.95 mM KCl, 1.25 mM NaH_2PO_4, 26 mM $NaHCO_3$, 0.5 mM $CaCl_2$, 10 mM $MgSO_4$, 10 mM D-glucose, and 3 mM kynurenic acid and were bubbled with 95% O_2/5% CO_2 (330–340 mosmol^{-1}). Coronal (350-μm-thick) slices were cut using a vibratome. The slices were then incubated at −33 °C in ACSF containing 126 mM NaCl, 2.5 mM KCl, 26 mM $NaHCO_3$, 1.25 mM NaH_2PO_4, 2 mM $CaCl_2$, 10 mM D-glucose, and 2 mM $MgCl_2$ saturated with 95% O_2/5% CO_2 (pH 7.4, 300–310 mosmol^{-1}) for a minimum of 1 h before experimentation. Hippocampal slices were viewed on a fixed-stage upright microscope (Nikon FN-1) with a 40× water immersion objective equipped with differential interference contrast/infrared (DIC/IR) optics. Slices were maintained at 32 °C and gravity-superfused with ACSF solution throughout experimentation. For current-clamp recordings in S408/9A mice, slices were incubated in ACSF in the absence of kynurenic acid. Input/output curves were produced as previously described from DGGCs (28). Briefly, visually identified DGGCs were injected with 0.5-s square wave current injections from 20 to 300 pA in 20-pA increments.

For voltage-clamp recordings, the internal pipette solution contained 140 mM CsCl, 1 mM $MgCl_2$, 0.1 mM EGTA, 10 mM Hepes, 2 mM Mg-ATP, 4 mM NaCl, and 0.3 mM Na-GTP (pH 7.25, 280–290 mosM). Series resistance and whole-cell capacitance were continually monitored throughout the experiment. After these parameters had stabilized for a minimum of 5 min, synaptic currents were recorded using an Axopatch 200B amplifier (Molecular Devices), filtered at 2 kHz, sampled at 20 kHz, digitized (Digidata 1320A; Molecular Devices), and stored for off-line analysis (Minianalysis; Synaptosoft, Inc.). Access resistance of 10–20 MΩ (~80% compensation) was monitored using a voltage step of −5 mV, and data from cells were discarded when >20% change occurred.

sIPSCs were analyzed using pClamp 9.2 (Clampfit; Axon Instruments) and MiniAnalysis software using pooled population data expressed as the mean ± SEM. The decay phase was fitted with a monoexponential function (τ decay), and rise time was analyzed by comparing the mean with 10–90% rise time. Tonic current was calculated as the difference between the holding current before and after application of the indicated $GABA_AR$ antagonist (≥200 μM SR95531 or 100 μM picrotoxin). The mean holding current of a 10-ms epoch was sampled every 100 ms for a single data point, and a Gaussian fit was applied to the resulting all-points histogram. Epochs containing synaptic events or an unstable baseline were excluded from the analysis. Input/output curves were fitted with a Boltzmann function: $f(W) = \text{Max}/(1 + \exp[(I - I_{50})/k])$, where Max = maximum response, k = slope, and I_{50} = amplitude of current that produces 50% of the maximum response.

Fear Conditioning. Fear conditioning was carried out in a single chamber with foot-shock bars. For conditioning and context testing, the chamber walls were covered with patterned panels. The conditioning procedures were a 180-s baseline period, followed by two trials separated by 120-s intervals. For each trial, a 15-s 70-dB tone was played, which terminated with the application of a 1.5-mA foot shock during the last 1 s. Twenty-four hours later, context-dependent memory was assessed by placing the mice in the chambers containing the patterned panels (conditioning environment). The amount of time the mice spent freezing during the trials was digitally tracked and analyzed. Two hours after context testing, cue-dependent memory was assessed by placing the mouse in a chamber without the patterned panels and measuring the amount of time it spent freezing during a 120-s baseline period, followed by two 70-dB tones played for 15 s separated from one another by 60-s intervals.

Open-Field Test. Following a thorough cleaning of the arena with 70% (vol/vol) ethanol, individual mice were placed in the center of a 40 × 40-cm arena and movement was digitally tracked (EthoVision XT 7.0; Noldus Technology). Time spent in a predefined center arena and total distance traveled were calculated.

Light/Dark Box Assay. Following a thorough cleaning with 70% (vol/vol) ethanol of the two equally sized chambers (each chamber is 21 × 21 cm), individual mice were placed in the dark chamber and allowed to roam freely between the dark and light chambers. Movement and time spent in the different chambers were digitally tracked and calculated (EthoVision XT 7.0).

Marble Burying. Mice were transferred into a new cage with 6-inch deep bedding, and 20 glass marbles were placed evenly spaced apart in a 4 × 5 pattern on its surface. Mice were individually placed in the cage, and the number of marbles buried to two-thirds of their depth after 30 min was counted.

Two-Choice Social Assay. In the two-choice assay, the subject mouse is placed at the bottom of a T-shaped container made of Plexiglas with two perpendicular arms (the long arm is 63.5 × 10 cm, and each short arm is 55 × 10 cm, surrounded by 32-cm high walls). All chambers and wire cups were cleaned with 70% (vol/vol) ethanol between each subject mice. The first session is a habituation period, where the subject mouse was able to roam freely across the three arms. This session was followed by a testing session, where a novel object (empty cup) was placed in the left arm or a novel mouse (stranger mouse under the wire cup) was placed in the right arm. The subject mouse was able to move freely across all three arms, and the cumulative time spent in the left arm or right arm was digitally tracked and quantified (EthoVision XT 7.1; Noldus Technology).

Social Novelty. Briefly, on the first day of training, mice were exposed to the open-field arena (40 × 40 cm) for 10 min. On the second day of training, mice were placed in an empty open-field arena for 5 min, followed by 5 min of exposure to two empty cages. On the third day, testing for social novelty was carried out by placing the subject mouse in an empty open-field arena for 5 min, followed by another 5 min when an empty cage (familiar object) or a novel object (empty salt shaker) was placed in opposite corners of the open-field arena. The amount of time the mice spent exploring in a predefined zone around the objects was digitally tracked (EthoVision XT 7.0).

Three-Chamber Social Test. Briefly, we constructed a three-chamber apparatus with Plexiglas containing three equally sized chambers (30 × 30 cm); two doors that can be remotely opened separate the middle chamber from the left and right chambers. A wire cup (4-inch diameter; item no. 010591315704, organizeit.com) was used as the empty cage or housed a stranger mouse (novel mouse), and the sniff zone 5 cm from the center of the wire cup was predefined. All chambers and wire cups were cleaned with 70% (vol/vol) ethanol between subject mice. A 10-min habituation period where the subject mouse was placed in the center chamber with the doors to the other chambers closed was followed by another 10-min session where the subject mouse was able to roam freely across all three chambers. These sessions were followed by a third 10-min session where a novel object (empty cup) was placed in the left chamber or a novel mouse (stranger mouse under the wire cup) was placed in the right chamber. The subject mouse was freely able to move across all three chambers, and the amount of time it spent in the predefined sniff zone (5-cm radius proximal to each cage) was

digitally monitored (EthoVision XT 7.1). A fourth 10-min session was used to test for social novelty, where a second stranger mouse was placed in the previously empty cage. The subject mouse was then able to roam freely across all three chambers, with the right chamber holding the previously encountered mouse (familiar mouse) and the left chamber holding the novel mouse (stranger mouse). Cumulative time spent in the left or right sniffing zone was digitally tracked and quantified. (EthoVision XT 7.1).

Golgi Staining. For Golgi staining, we used the protocol recommended by the manufacturer of the FD Rapid GolgiStain Kit (FD NeuroTechnologies, Inc.). Briefly, mice were deeply anesthetized, and brains were rapidly extracted and rinsed in Milli-Q water generated at Tufts University within the S.J.M. laboratory. Brains were immersed in the provided solutions for 14 d at room temperature in the dark. Following Golgi–Cox immersion, 200-μm-thick coronal sections were prepared on a vibratome. Sections were then developed according to the manufacturer's protocol and dehydrated in 50%, 75%, 95%, and absolute ethanol; cleared in xylene; and coverslipped with Permount (catalog no. SP15; Thermo Fisher Scientific). Dendritic spine analysis was performed on dendritic spines located immediately adjacent to the DGGC layer in the molecular layer of the hippocampus using images collected with a 60× objective (Nikon). Spine density in 30-μm-long sections was calculated.

Statistical Analysis. All data are presented as the mean ± SEM and were analyzed with the Student's *t* test, one-way ANOVA with Turkey's multiple comparison test, and two-way ANOVA with Bonferroni's post hoc comparison. Unless otherwise indicated, $P < 0.05$ was considered statistically significant. All analyses were done using Prism 6 (GraphPad).

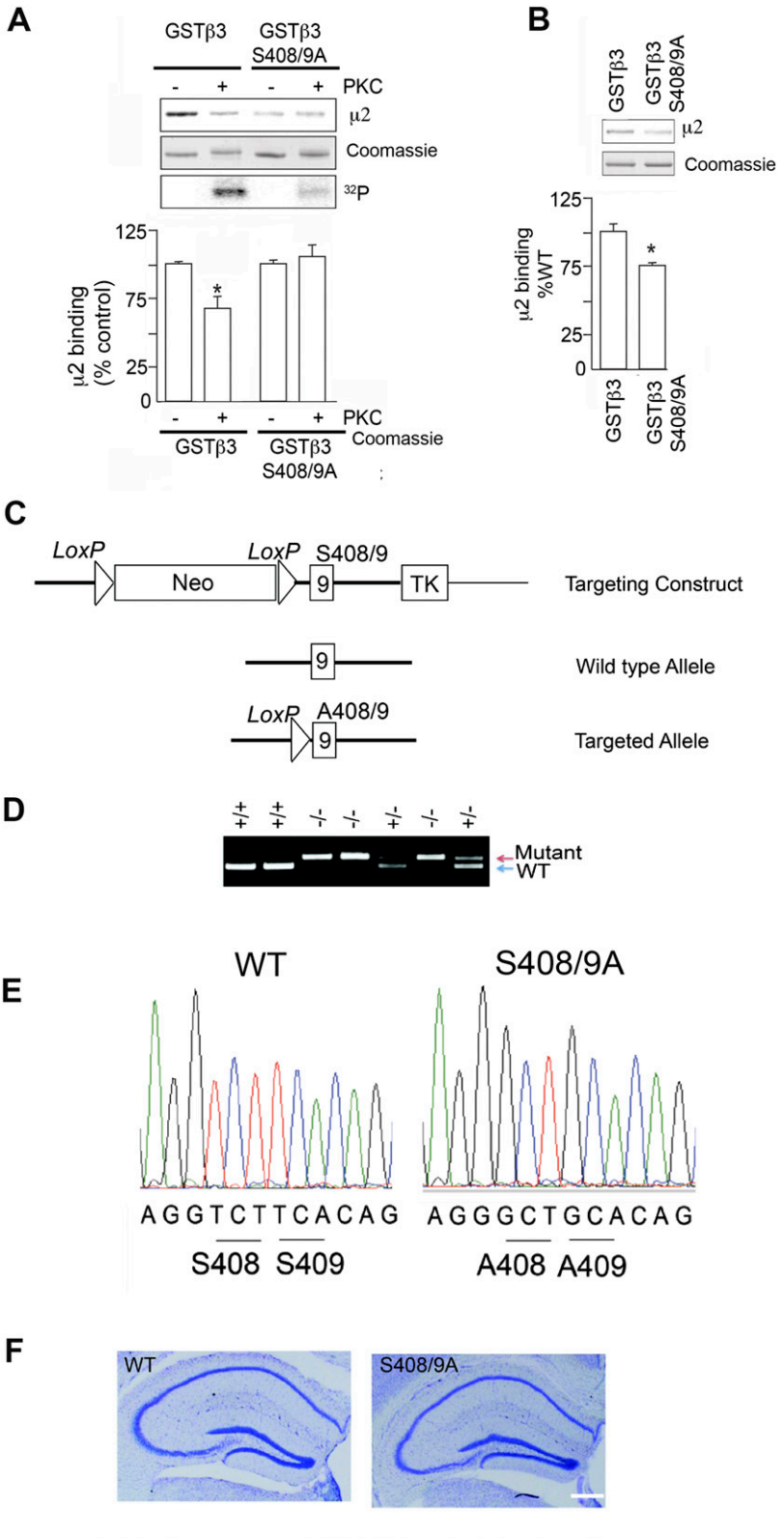

Fig. S1. Characterization of β3 phosphorylation and generation of S408/9A mice. (*A*) GST fusion proteins encoding the major intracellular domain of the β3 subunit (GST-β3) and a mutant fusion protein in which residues S408/9 were mutated to alanines (GSTβ3S408/9A) were purified from *E. coli*. Fusion proteins were subjected to in vitro phosphorylation using purified PKC. GSTβ3 was phosphorylated to 0.35 mol/mol, and GSTβ3S4089A was purified to 0.03 mol/mol. Phosphorylated fusion proteins were then exposed to brain lysates and immunoblotted with μ2 antibodies. Coomassie staining of the respective samples and an autoradiogram of samples exposed to ^{32}P–γ-ATP and PKC are shown. The level of μ2 binding was normalized to fusion proteins that had been incubated with heat-inactivated PKC. (*B*) AP2 binding to GSTβ3 and GSTβ3S408/9A was directly compared as outlined above. (*C*) Schematic diagram of the targeting

Legend continued on following page

construct for generating β3 S408/9A knock-in mice. The β3 S408/9A mice were generated by homologous recombination in ES cells. A targeting plasmid was constructed that contained a floxed neomycin (Neo) selection cassette in intron 8 of β3 genomic DNA and a flanking thymidine kinase-negative selection marker (TK). (*D*) Following Cre-mediated excision of the selection cassette in vivo, the presence of the mutant codons in exon 9 was confirmed by DNA sequencing. (*E*) PCR product of WT and β3 S408/9A DNA samples detecting the presence or absence of the remaining loxP site. (*F*) No gross morphological changes were observed in the hippocampus between WT and S408/9A mice as determined by Nissl staining. (Scale bar: 100 μm.)

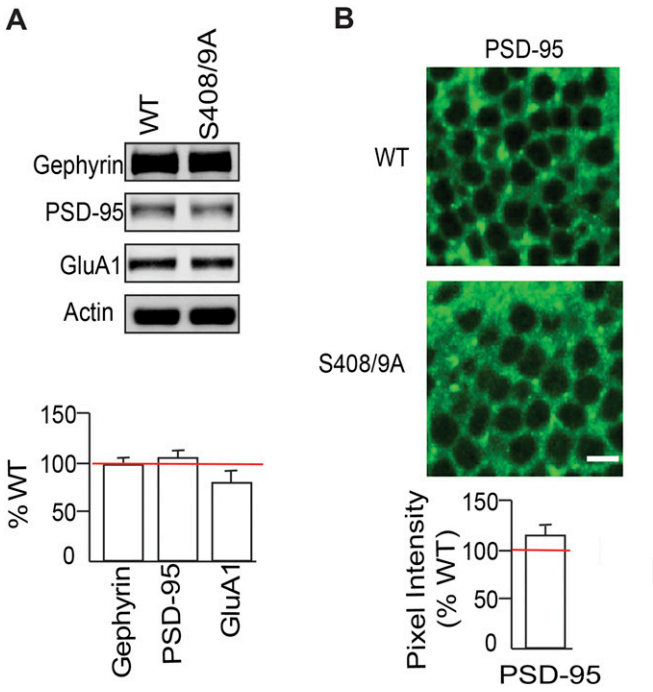

Fig. S2. Analyzing glutamate receptor expression in S408/9A mice. (*A*) Postsynaptic protein expression is unaltered in S408/9A mice. To determine whether the observed changes in inhibitory synapses were associated with alterations in postsynaptic proteins, the total expression of the inhibitory synaptic marker gephyrin, excitatory synaptic marker PSD-95, and AMPA receptor GluA1 were measured. Hippocampal lysates from S408/9A and WT control mice were subjected to SDS/PAGE and immunoblotted with gephyrin, PSD-95, and GluA1 antibodies. Protein expression in S408/9A mice was normalized to WT controls (100%; red line). No significant differences in postsynaptic protein expression were observed ($P > 0.05$, *t* test; $n = 8$ mice of each genotype). (*B*) Forty-micron hippocampal slices were stained with antibodies against the postsynaptic protein PSD-95, followed by confocal microscopy. The pixel intensity of PSD-95 staining was then compared within the dentate gyrus between genotypes. Preventing phosphorylation of the β3 subunit does not alter PSD-95 immunoreactivity ($P > 0.05$, *t* test; $n = 8$ mice of each genotype). (Scale bar: 10 μm.)

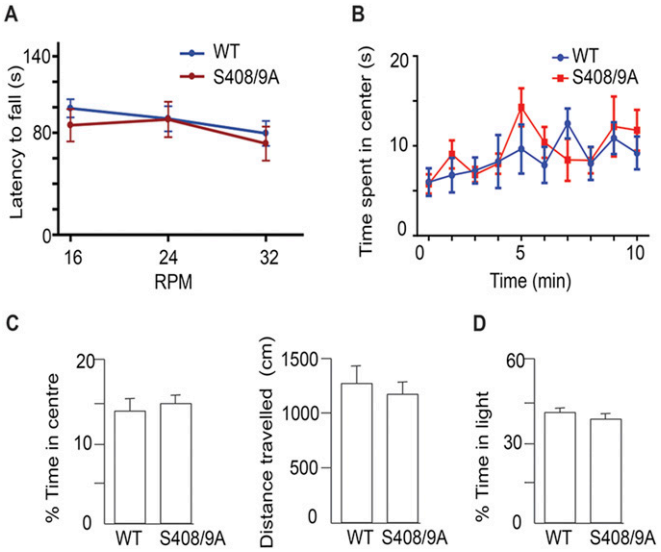

Fig. S3. Characterization of motor activity and anxiety-like behavior in S408/9A mice. (*A*) Locomotor activity of WT and S408/9A mice was examined using the rotarod test, and the latency to fall was determined. There were no significant differences in motor activity ($P > 0.05$, *t* test; $n = 10–11$ mice of each genotype). RPM, revolutions per minute. (*B*) Time spent in the center of the arena in an open field was compared for WT and S408/9A mice over a 10-min time course. (*C*) In the open-field assay, there were no significant differences in the percentage of time spent in the middle of the open-field arena or in the distance traveled between genotypes ($P > 0.05$, *t* test; $n = 12$ mice of each genotype). (*D*) Percentage of time spent in the light arena of the light/dark box assay was determined for WT and S408/9A mice. There were no significant differences in the percentage of time spent in the light arena between genotypes ($P > 0.05$, *t* test; $n = 12$ mice of each genotype).

Table S1. Comparing the excitability of DGGCs between genotypes

No. of action potentials fired in DGGCs	WT	S408/9A
Current injection amplitude, pA		
20	0.4 ± 0.4	0.0 ± 0.0
40	0.6 ± 0.5	1.0 ± 0.8
60	4.3 ± 1.8	6.9 ± 2.5
80	10.9 ± 2.9	17.1 ± 4.2
100	21.5 ± 3.5	24.5 ± 4.4
120	30.9 ± 3.6	34.0 ± 4.7
140	39.1 ± 3.6	42.6 ± 5.1
160	46.8 ± 3.8	49.7 ± 5.4
180	55.6 ± 3.8	57.9 ± 5.6
200	63.5 ± 4.3	65.0 ± 5.8
220	71.5 ± 4.6	72.2 ± 5.9
240	80.7 ± 4.7	77.5 ± 6.1
260	87.8 ± 4.9	83.2 ± 6.1
280	94.4 ± 5.0	89.5 ± 6.5
300	100.0 ± 4.9	93.6 ± 6.6
RMP, mV	−81.8 ± 1.2	−81.3 ± 1.2
I_{50}, pA	169.0	164.2
k	48.0	51.9
n	19	20

Values are mean ± SE. I_{50}, amplitude of current injection eliciting 50% of maximum response; *k*, slope factor; *n*, number of mice; RMP, resting membrane potential.